Electronic Supplementary Material (ESI) for ChemComm.

Supporting Information

Modulated synthesis of hcp MOFs for preferential CO_2 capture

Jiaxi Zhang,[a] Mehak Nawaz Khan,[a] Zhigang Hu,*[a] Jianxin Zou*[a]

[a] Shanghai Key Laboratory of Hydrogen Science & Center of Hydrogen Science, School of Materials Science and Engineering, Shanghai Jiao Tong University, Shanghai, 200240, China

Correspondence to: zhigang.hu@sjtu.edu.cn or zoujx@sjtu.edu.cn

Experimental Section

Materials and Methods

All the reagents were obtained from commercial suppliers and used without further purification. Powder X-ray diffraction (PXRD) patterns were obtained on a Mini Flex 600 X-ray diffractometer equipped with a Cu-sealed tube (λ = 1.54178 Å) at the scan rate of 0.02 degree/s. Scanning electron microscope (SEM) analyses were conducted on a TESCAN MANGA (UH-resolution mode) equipped with an energy-dispersive spectrometer (EDS, Triglave TM). Samples were treated via Pt sputtering (Q 150T ES plus) before observation. Atomic force microscope (AFM) analyses were conducted on a Bruker Dimension Icon with samples dispersing on mica sheets. Thermogravimetric analysis (TGA) was performed using a TGA8000 thermal analyzer under a flowing N_2 gas (100 mL/min) with a heating rate of 10 ℃ min^{-1}.

Modulated Hydrothermal (MHT) Synthesis of hcp-UiO-66-X MOFs

In a typical process,[1-4] $Zr(NO_3)_4 \cdot 5H_2O$ (2.232 g, ~5.2 mmol) and terephthalic acid ligand (0.831 g, ~5 mmol) were orderly suspended in 50 mL of acetic acid (modulator)/water mixed solvent with various ligand/modulator (L/M) molar ratios of 0.007 eq., 0.015 eq., 0.029 eq., and 0.059 eq. The mixed solution was then transferred to a heating reflux device and reacted at 120 ℃ for 12 h to yield a white emulsion. After configuration of the emulsion, the white powder product obtained was immersed in deionized water (DI water) and anhydrous methanol (MeOH) for three days at room temperature, during which the extract was decanted and DI water as well as MeOH was added every day.

Solvothermal Synthesis of UiO-66

The solvothermal synthesis of fcu UiO-66 was based on the modification of a reported procedure. [5] Briefly, benzene-1,4-dicarboxylic acid (BDC) (0.83 g, ~5 mmol) and $ZrCl_4$ (1.21 g, ~5.2 mmol) dissolved in 20 mL of dimethylformamide (DMF)/formic acid (18/2, v/v) mixed solvent were loaded into a Teflon-lined autoclave and heated at 120 ℃ for 12 h. The product was soaked in anhydrous methanol for 3 days at room temperature, during which time the extract was decanted and fresh methanol was added every day. Then the sample was treated with deionized water similarly for another 3 days. This process was carried out to wash out residual reagents trapped inside the pores. After removal of water by decanting, the sample was dried under a dynamic vacuum at 120 ℃ for overnight to afford the final product.

Gas Sorption Measurements

Gas sorption isotherms of hcp-UiO-66 MOFs were measured up to 1 bar using Micrometirics ASAP 2020 surface area and pore size analyzer. Before measurements, the samples (~100 mg) were degassed under reduced pressure ($<10^{-2}$ Pa) at 120 ℃ for 12 h. UHP-grade CO_2 and N_2 ($\geq$ 99.9999%) were used for gas sorption measurements. Oil-free vacuum pumps and oil-free pressure regulators were used to prevent

contamination of the samples during the degassing process and isotherm measurements. The temperature of 77 K, 273 K and 298 K were maintained with a liquid nitrogen bath, and ice water bath, and 298 K water bath, respectively. Pore size distribution data were calculated from the N_2 adsorption isotherms at 77 K based on the nonlocal density functional theory (NLDFT) model in the Micromeritics ASAP 2020 Plus software package (assuming slit pore geometry).

Calculations of isosteric heat of adsorption (Qst) [6]

The CO_2 adsorption isotherms measured at 273 K and 298 K were first fitted to a virial equation (Equation 1). The fitting parameters were then used to calculate the isosteric heat of adsorption (Q_{st}) using Equation 2,

$$ln\,P = ln\,N + \frac{1}{T}\sum_{i=0}^{m} a_i N^i + \sum_{i=0}^{n} b_i N^i \quad (1)$$

$$Q_{st} = -R\sum_{i=0}^{m} a_i N^i \quad (2)$$

where P is pressure (mmHg), N is adsorbed quantity (mmol g^{-1}), T is temperature (K), R is gas constant (8.314 J K^{-1} mol^{-1}), a_i and b_i are virial coefficients, m and n represent the number of coefficients required to adequately describe the isotherms (herein, m = 5, n = 2).

Gas selectivity calculated using ideal adsorption solution theory (IAST) [7]

The CO_2 and N_2 adsorption isotherms were first fitted to a dual-site Langmuir-Freundlich (DSLF) model (Equation 3),

$$cq = \frac{q_{sat,A} b_A p^{v_A}}{1+b_A p^{v_A}} + \frac{q_{sat,B} b_B p^{v_B}}{1+b_B p^{v_B}} \quad (3)$$

where q is the amount of adsorbed gas (mmol g^{-1}), p is the bulk gas phase pressure (bar), q_{sat} is the saturation amount (mmol g^{-1}), b is the Langmuir-Freundlich parameter ($bar^{-\alpha}$), v is the Langmuir-Freundlich exponent (dimensionless) for two adsorption sites A and B indicating the presence of weak and strong adsorption sites.

IAST starts from the Raoults' Law type of relationship between fluid and adsorbed phase,

$$P_i = P y_i = P_i^o x_i \quad (4)$$

$$\sum_{i=1}^{n} x_i = \sum_{i=1}^{n} \frac{P_i}{P_i^0} = 1 \quad (5)$$

where P_i is partial pressure of component i (bar), P is total pressure (bar), y_i and x_i represent mole fractions of component i in gas and adsorbed phase (dimensionless), respectively. P_i^0 is equilibrium vapour pressure (bar).

In IAST, P_i^0 is defined by relating to spreading pressure π,

$$\frac{\pi S}{RT} = \int_0^{P_i^0} \frac{q_i(P_i)}{P_i} dP_i = \Pi \text{ (Constant)} \quad (6)$$

where π is spreading pressure, S is specific surface area of adsorbent (m^2 g^{-1}), R is gas constant (8.314 J

K^{-1} mol^{-1}), T is temperature (K), $q_i(P_i)$ is the single component equilibrium obtained from isotherm (mmol g^{-1}).

For a DSLF model, the analytical expression for the integral is derived as:

$$c\int_0^{P_i^0} \frac{q_i(P_i)}{P_i} dP_i = \Pi \text{ (Constant)} = \frac{q_{sat,A}}{\alpha_A} ln[1 + b_A(P_i^0)^{\alpha_A}] + \frac{q_{sat,B}}{\alpha_B} ln[1 + b_B(P_i^0)^{\alpha_B}] \quad (7)$$

The isotherm parameters are derived from the previous fitting. For a binary component system, the unknowns will be Π, P_1^0, and P_2^0 which can be obtained by simultaneously solving Equations 5 and 7.

The adsorbed amount for each compound in a mixture is

$$q_i^{mix} = x_i q_T \quad (8)$$

$$\frac{1}{q_T} = \sum_{i=1}^{n} \frac{x_i}{q_i(P_i^o)} \quad (9)$$

where q_i^{mix} is the adsorbed amount of component i (mmol g^{-1}), q_T is the total adsorbed amount (mmol g^{-1}). The adsorption selectivities S_{ads} were calculated using Equation 10.

$$S_{ads} = \frac{q_1/q_2}{p_1/p_2} \quad (10)$$

Grand canonical Monte Carlo (GCMC) Simulation

All simulations were performed by the Materials Studio (MS) 2020 package. The preferred sorption locations were performed by GCMC simulations with Adsorption fixed loading task and Metropolis method [5] in the sorption calculation module. As for all of the GCMC simulations, the framework was considered to be rigid. The framework and gas molecule were described by the force filed of COMPASSIII. The cutoff radius was set to 10 Å, for the Lennard-Jones (LJ) interactions, and the electrostatic interactions, and the Ewald summation method was selected to calculate the electrostatic interactions between adsorbates as well as between adsorbates and the framework. For state point in GCMC simulation, the system adopted 1×10^6 Monte Carlo steps to guarantee equilibration, and the ultimate data was collected for another 1×10^6 Monte Carlo steps. The charges of the atoms of both gas molecules and the framework were assigned by the forcefiled of COMPASSIII. The details of physical characteristics of MOF materials calculated by using the N_2 probe with a radius of 1.82 Å in Zeo++ software. [6], [7]

Breakthrough Experiments

Breakthrough experiments were conducted using the home-built setup.[8] Breakthrough experiments were conducted using the home-built setup shown in Figure S11. Gas flow rates were regulated by mass flow controllers (Alicat Scientific). Before a typical breakthrough experiment, the column filled with adsorbent was activated by purging with a constant He flow [30 scc/min] at 298 K for 12 hours until no signal from solvent or moisture could be observed by the mass spectrometer (Hiden QGA quantitative gas analysis system). After that, an equimolar mixture of CO_2 and N_2 was introduced into the stainless-steel

column (10 cm) filled with hcp-UiO-66-0.015 (0.67 g) at a total flow rate of 20 ± 0.5 cc min^{-1}. The gas composition at the exit of the column was determined by mass spectrometry, and the flow rate of each component was calibrated by an internal Ar flow reference with a fixed flow rate of 5 ± 0.1 cc min^{-1}.

The mean residence time of gas components and the gas uptake of the packed adsorbent were calculated using the Equation 11:

$$\int_0^{t_C} \left[1 - \frac{v_t y_t}{v_t^{\infty} y_t^{\infty}}\right] dt = \bar{t} = \frac{L}{v_0}\left[\frac{P_{in}+P_{out}}{2P_{in}} + \left(\frac{1-\varepsilon}{\varepsilon}\right)\frac{q_e}{C_0}\right] \quad (11)$$

where ε is the bed porosity, v_0 is the interstitial gas velocity (cm s^{-1}) at the column inlet, C_0 is the inlet gas concentration (mmol cm^{-3}), A is the cross sectional area of column (cm^2), t_c is the elution time (s), v_t is the interstitial gas velocity (cm s^{-1}) at the exit of the column, C_t is the exit gas concentration (mmol cm^{-3}), C_e is the gas concentration at the average column pressure (mmol cm^{-3}), P_{in} and P_{out} are the inlet(upstream) and exit (downstream), respective1ly, L is the column length (cm), q_e is the equilibrium concentration of adsorbate in the adsorbent (mmol cm^{-3}) corresponding to the average column pressure.

The breakthrough selectivity was calculated as

$$s = \frac{(q_e/c_0)_{CO_2}}{(q_e/c_0)_{N_2}} \quad (12)$$

The breakthrough curves in this study are all presented after blank correction. The blank runs were conducted at conditions similar to the actual breakthrough tests. The mean residence time of the blank run was subtracted from the mean residence time of the actual breakthrough run.

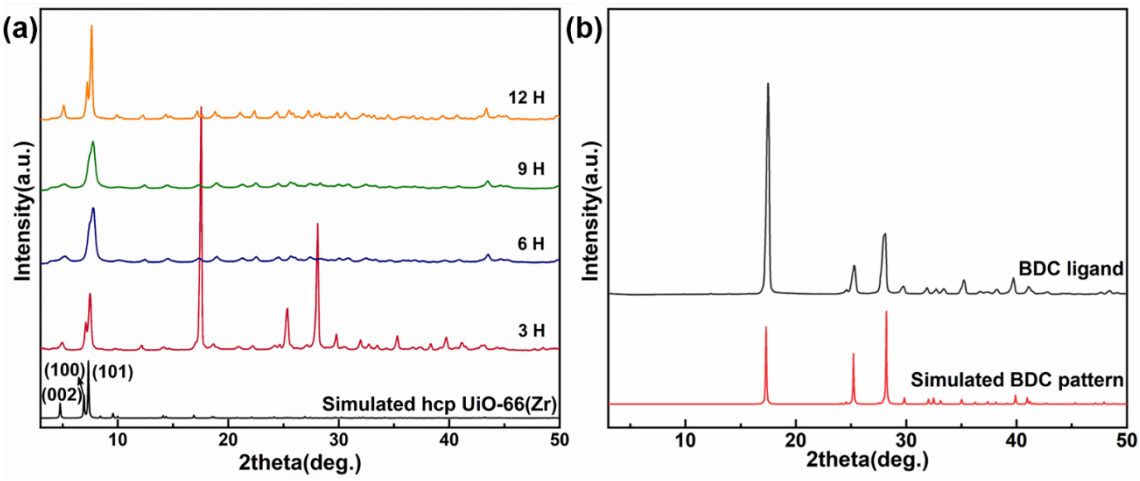

Figure S1. PXRD patterns of (a) hcp-UiO-66-0.015 at different reaction time and (b) BDC ligand.

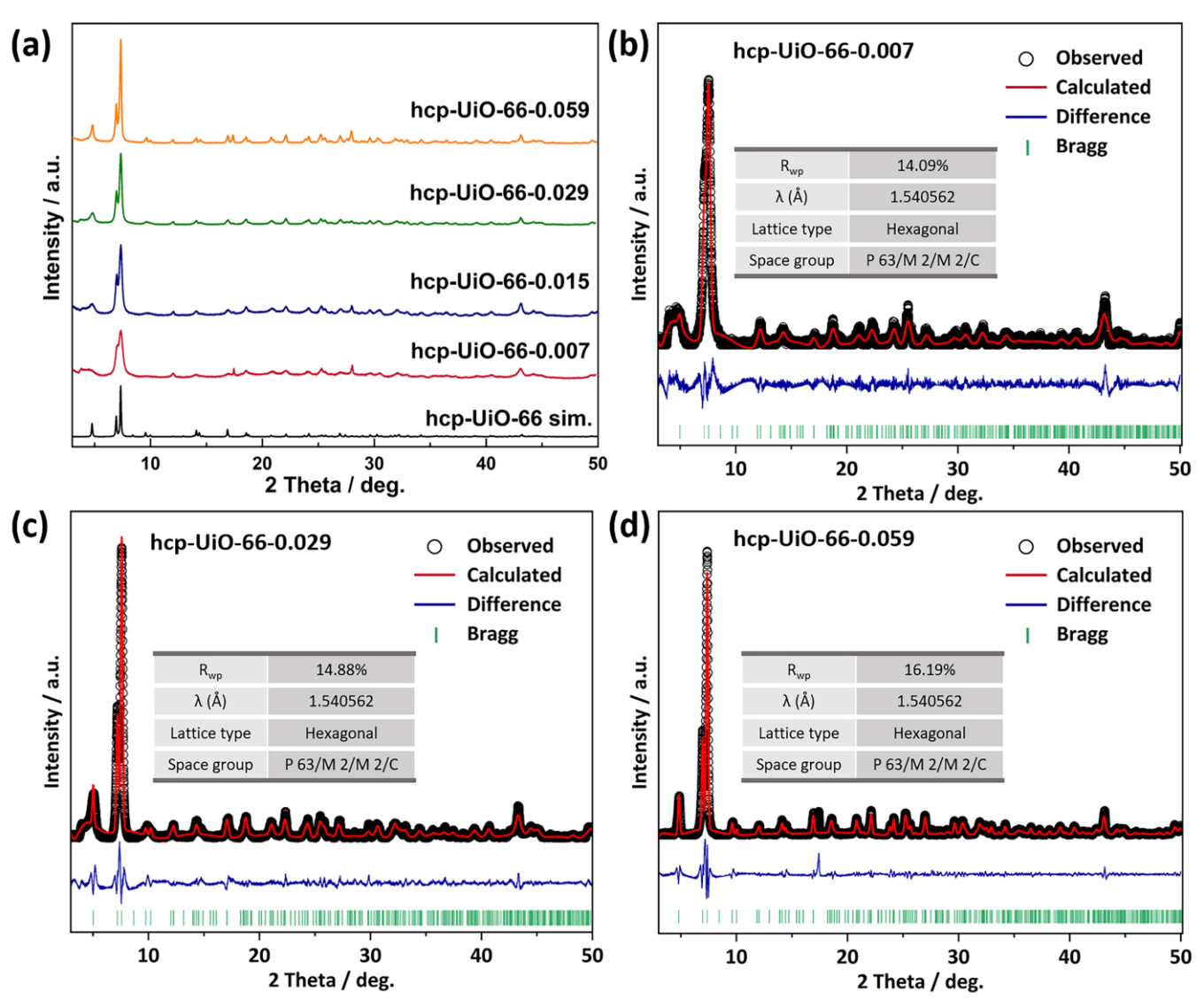

Figure S2. (a) PXRD patterns of the four hcp-UiO-66 MOFs and Pawley refinement XRD results of (b) hcp-UiO-66-0.007, (c) hcp-UiO-66-0.029 and (d) hcp-UiO-66-0.059.

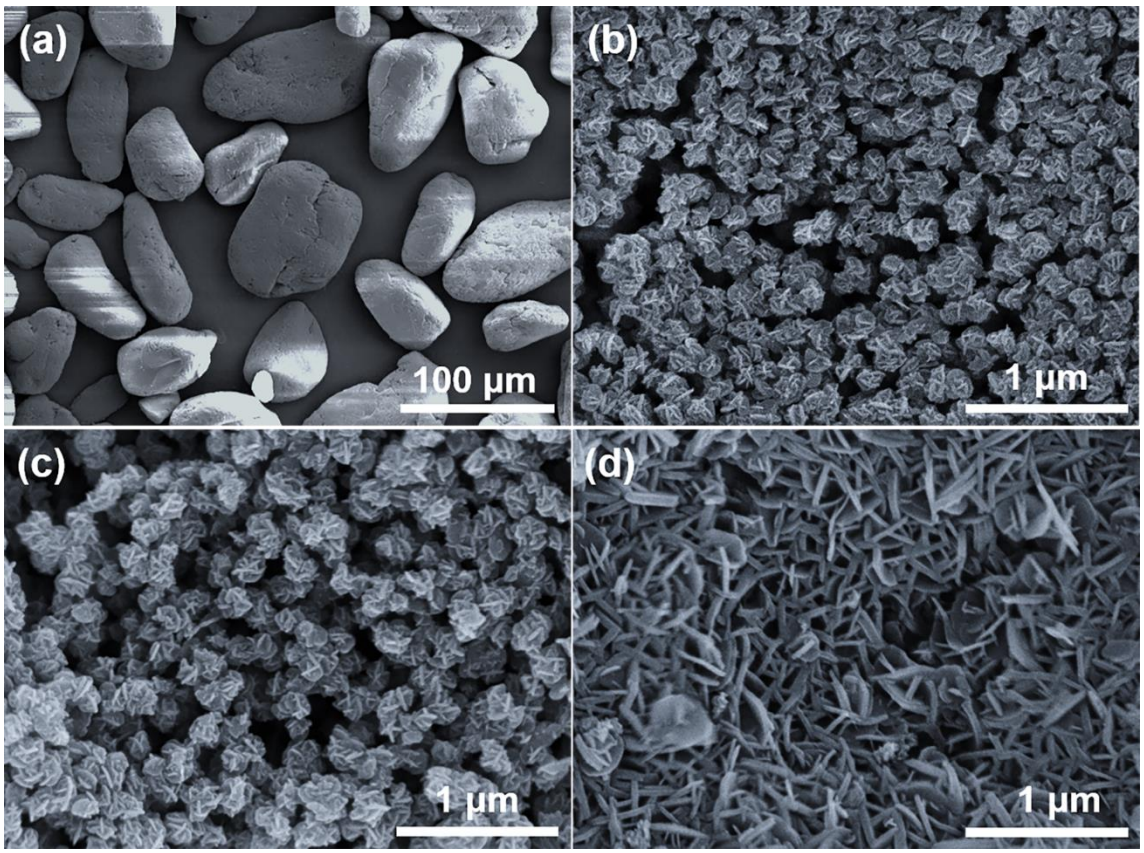

Figure S3. SEM images of hcp-UiO-66-0.015 at different reaction time: (a) 3 h, (b) 6 h, (c) 9 h, and (d) 12 h.

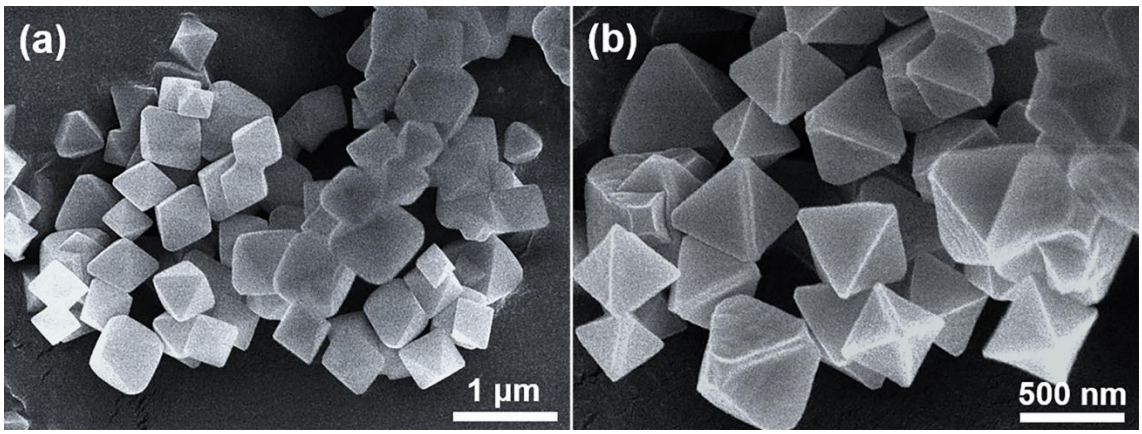

Figure S4. FESEM images of fcu UiO-66 by solvothermal method.

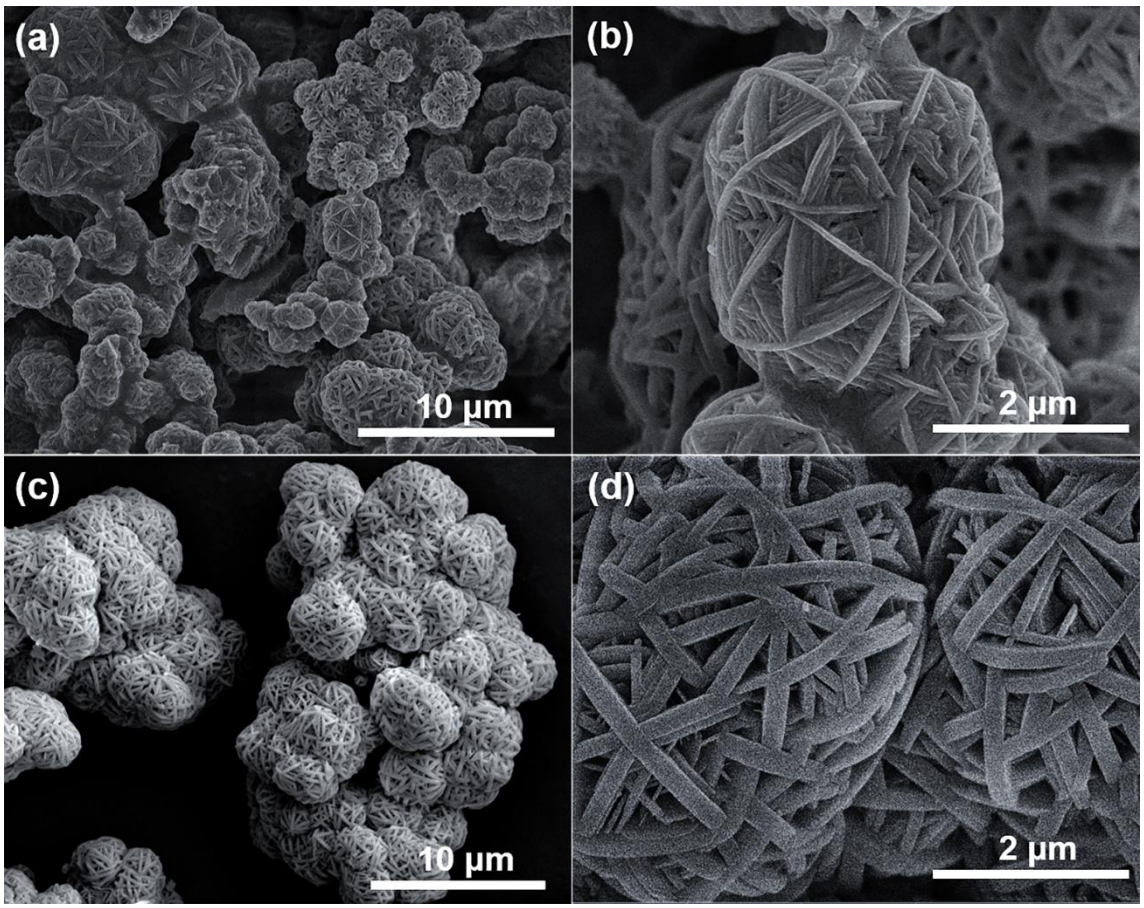

Figure S5. FESEM images of (a), (b) hcp-UiO-66-0.029 and (c), (d) hcp-UiO-66-0.059.

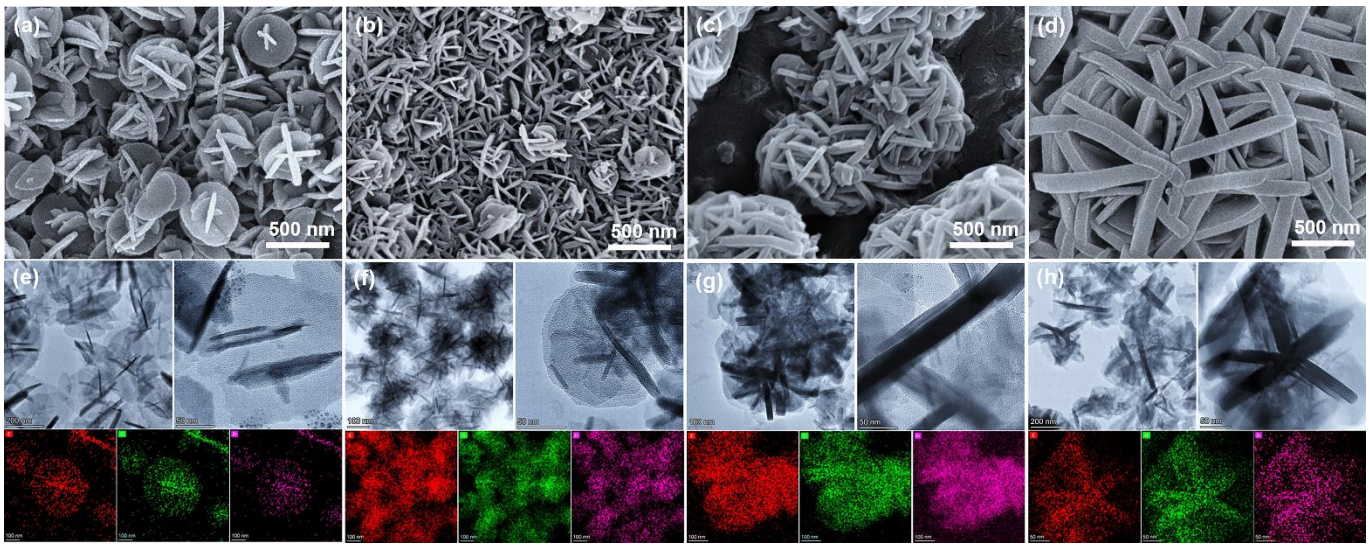

Figure S6. FESEM images of UiO-66 with different L/M eq.: (a) hcp-UiO-66-0.007, (b) hcp-UiO-66-0.015, (c) hcp-UiO-66-0.029, (d) hcp-UiO-66-0.059. TEM and EDS mapping images of UiO-66 with different L/M eq.: (e) hcp-UiO-66-0.007, (f) hcp-UiO-66-0.015, (g) hcp-UiO-66-0.029, (h) hcp-UiO-66-0.059.

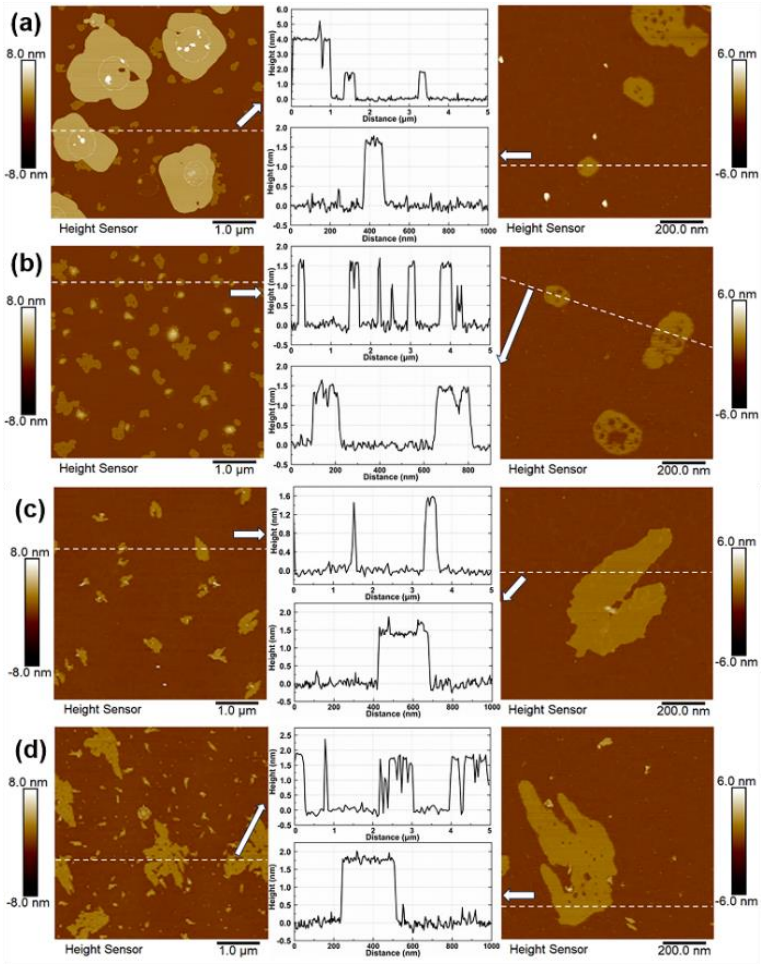

Figure S7. AFM images and corresponding thickness distribution curves of UiO-66 with different L/M eq.: (a) hcp-UiO-66-0.007, (b) hcp-UiO-66-0.015, (c) hcp-UiO-66-0.029, (d) hcp-UiO-66-0.059.

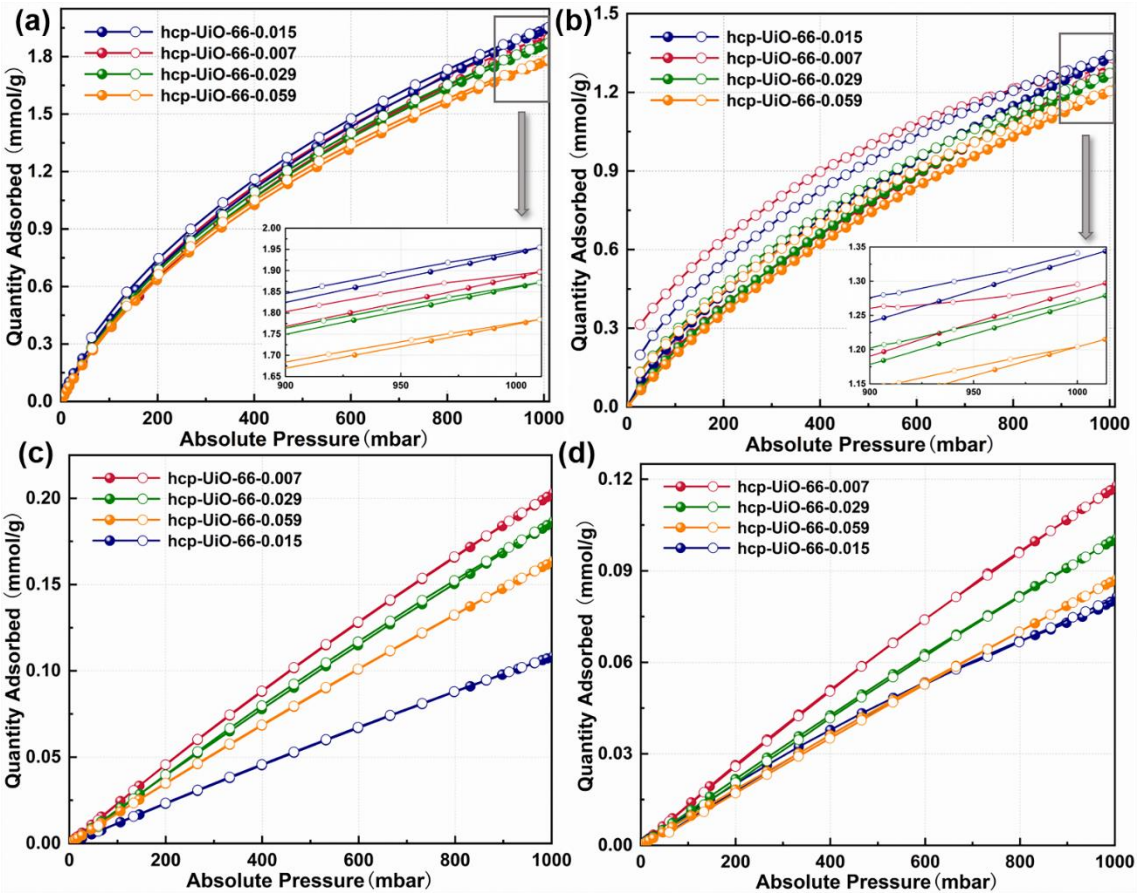

Figure S8. Gas isotherms of four hcp-UiO-66-X (filled, adsorption; open, desorption): (a) CO_2 at 273 K; (b) CO_2 at 298 K; (c) N_2 at 273 K; (d) N_2 at 298 K.

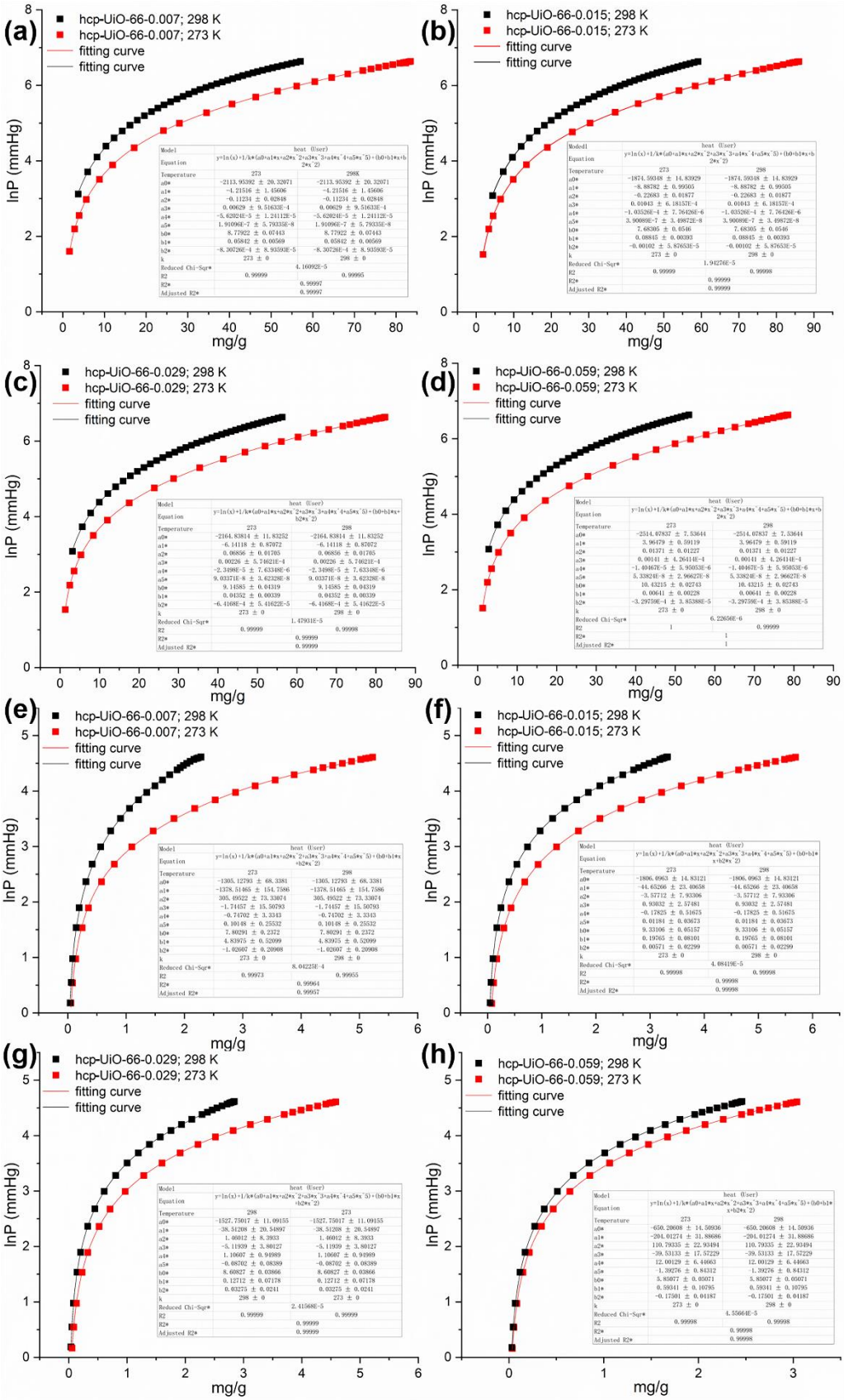

Figure S9. Parameter fittings for calculating the adsorption heats of hcp-UiO-66-X. (a), (b), (c), (d) CO_2 gas and (e), (f), (g), (h) N_2 gas.

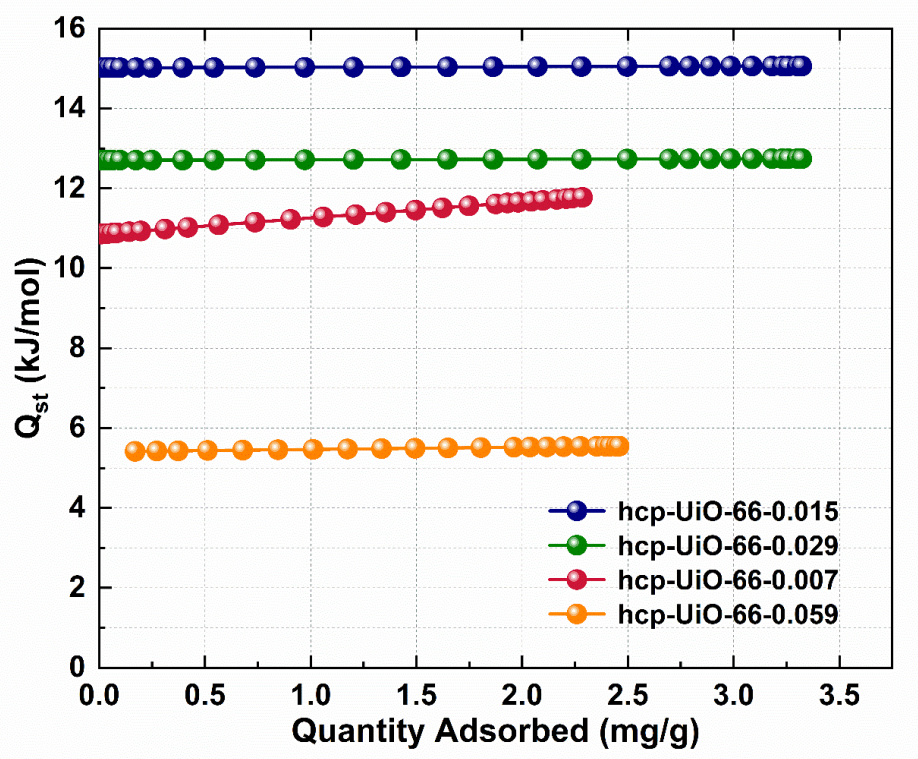

Figure S10. Q_{st} values of N_2 of the hcp-UiO-66 MOFs.

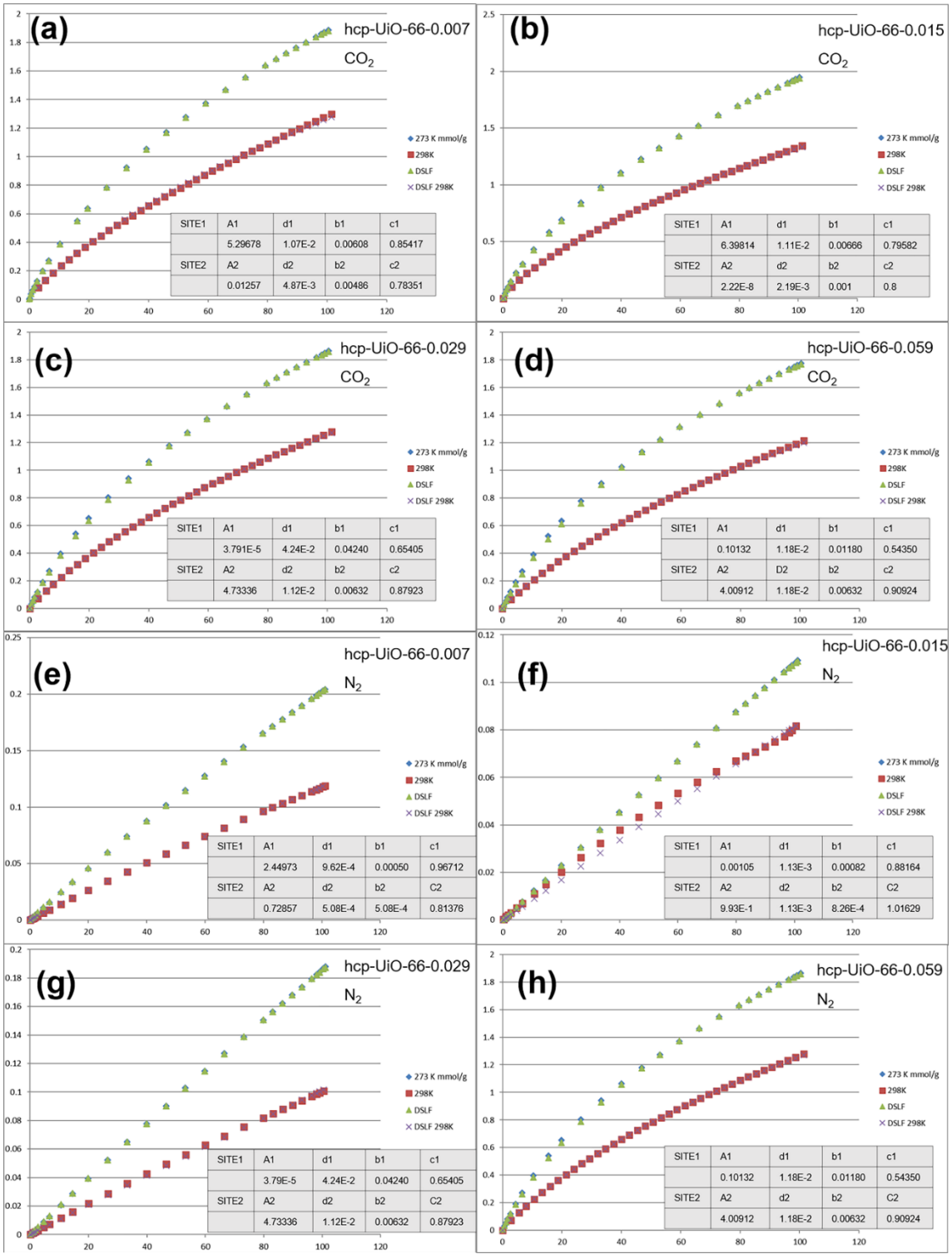

Figure S11. DLSF parameter fittings of hcp-UiO-66 MOFs: (a), (c), (e), (g) CO_2 gas; (b), (d), (f), (h) N_2 gas.

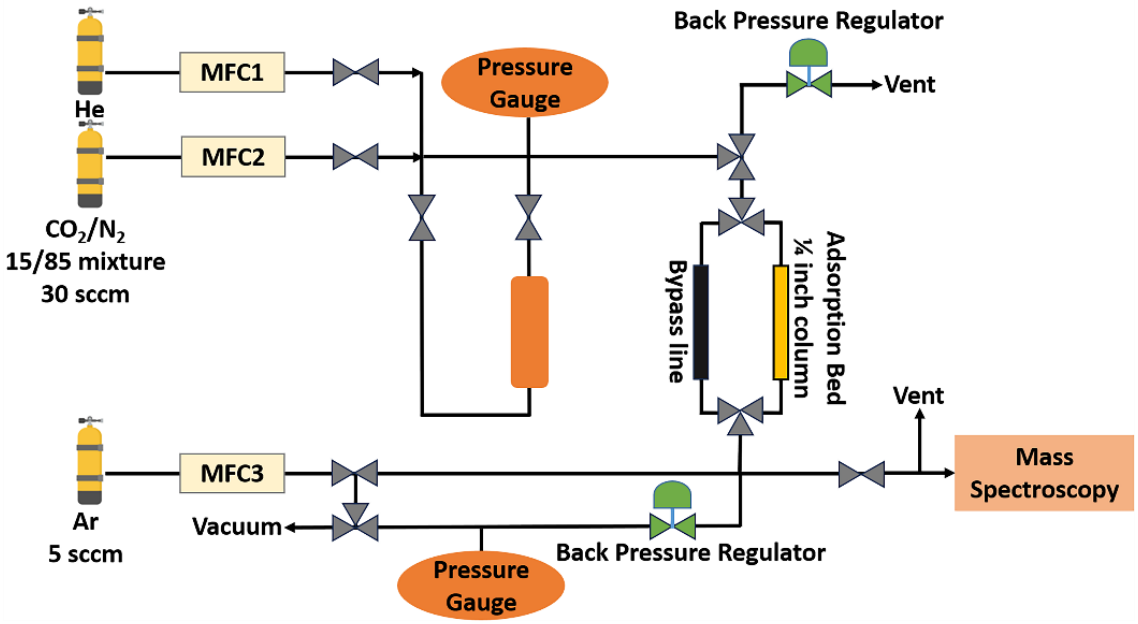

Figure S12. A scheme of the home-built breakthrough set-up used in this study.

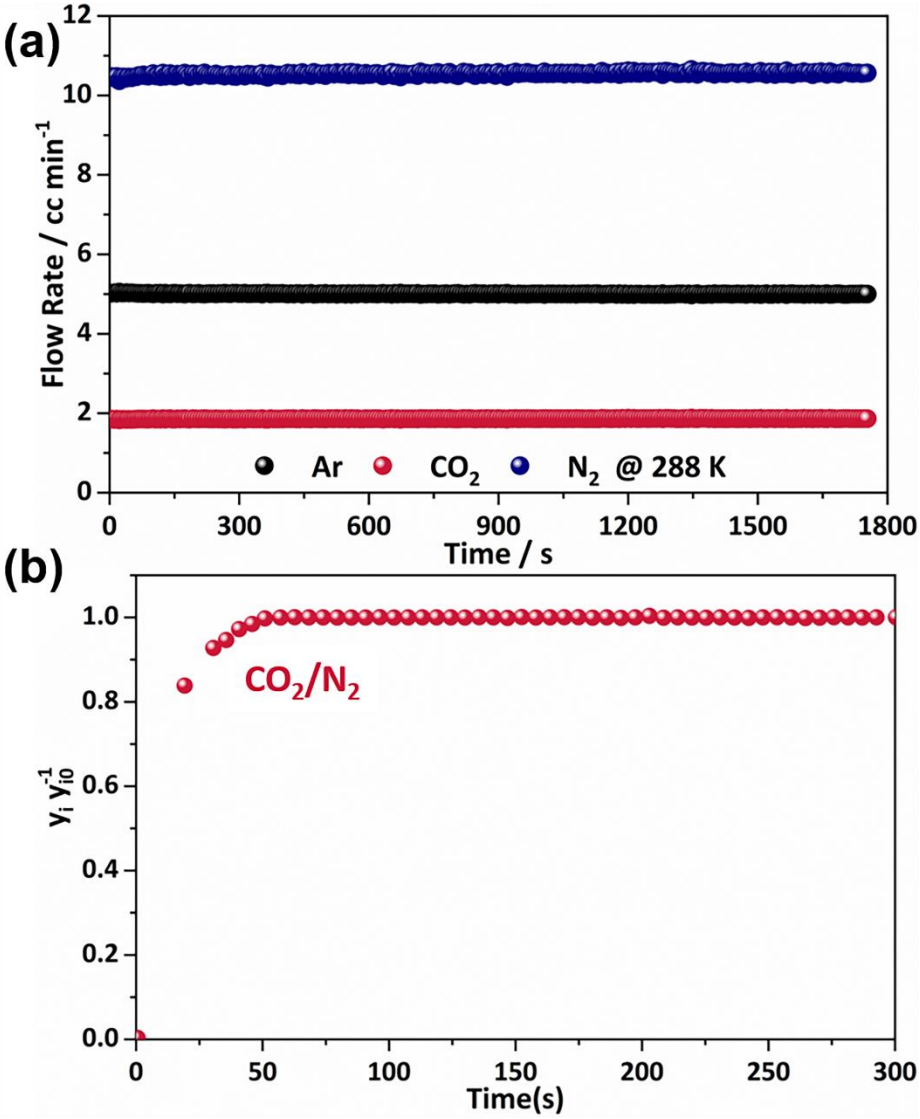

Figure S13. (a) Calibration of dry CO_2/N_2 binary mixtures using a fixed Ar flow (5 ± 0.1 cc min^{-1}, P = 1 bar) as an internal reference detected by mass spectrometer at 298 K. (b) Breakthrough curve of CO_2/N_2 binary mixtures running through a bypass gas line. The dead volume time of the gas mixture was hence calculated to be 55.7s.

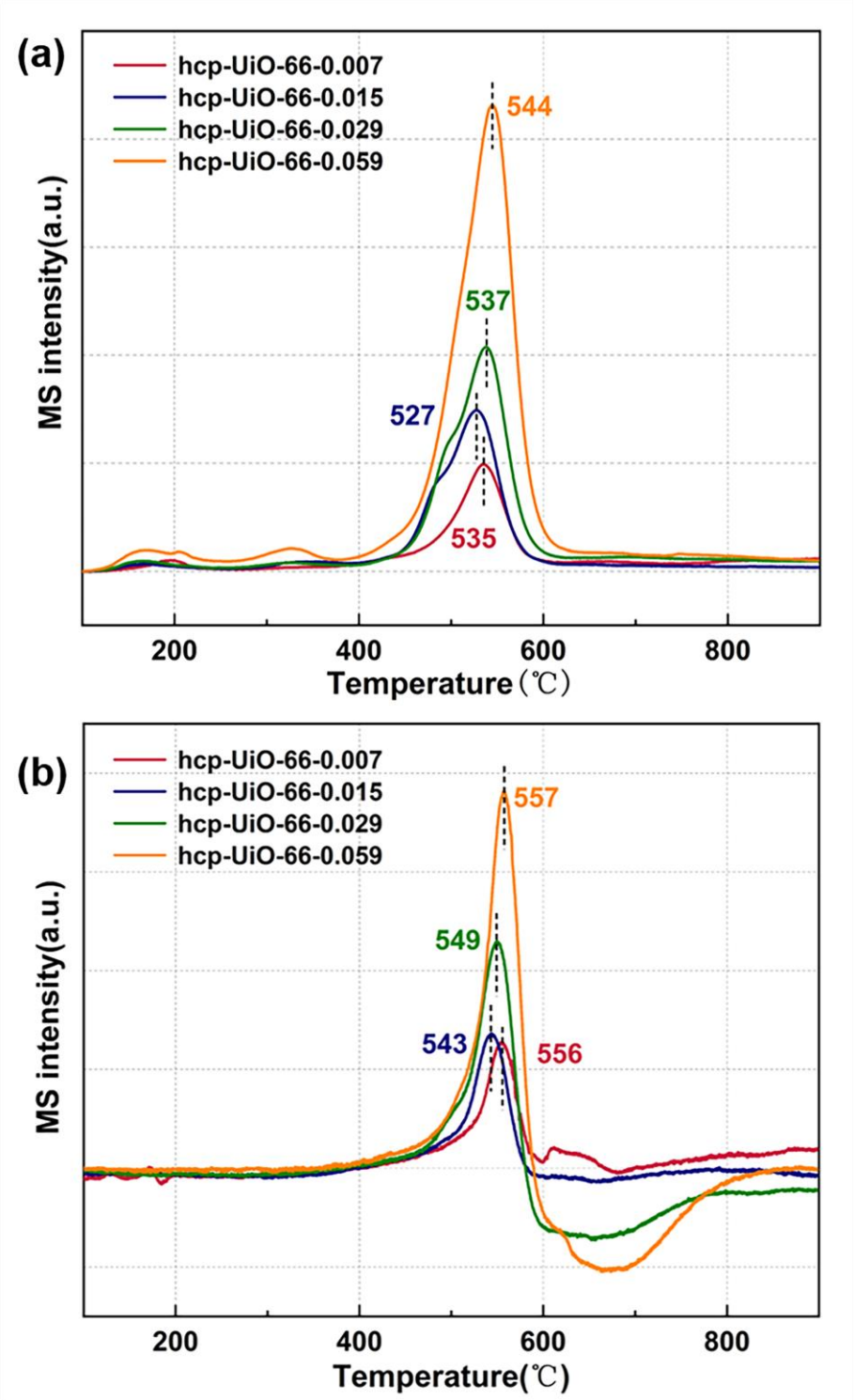

Figure S14. NH_3-TPD (a) and H_2-TPR (b) curves of hcp-UiO-66-X. (a)-(b) CO_2 binding sites of theoretical fcu-UiO-66 determined from the single-component CO_2 GCMC simulation at 1 bar and 298 K.

Table S1. Physical properties of hcp-UiO-66 MOFs.

	hcp-UiO-66-0.007	**hcp-UiO-66-0.015**	**hcp-UiO-66-0.029**	**hcp-UiO-66-0.059**
BET SA[a]	287	**759**	607	482
Pore volume[b]	0.05	**0.21**	0.18	0.15
CO_2 uptake at 298 K and 0.15 bar[c]	0.09	**0.34**	0.31	0.29
CO_2 uptake at 298 K and 1 bar[c]	0.50	1.35	1.18	1.15
Q_{st} of CO_2[d]	17.6	15.7	18.1	20.9
Q_{st} of N_2[d]	11.3	15.0	12.7	5.5
NH_3-TPD peak desorption temperature[e]	535	527	537	544
H_2-TPR peak reduction temperature[e]	556	543	549	557
IAST CO_2/N_2 (15/85) selectivity at 1 bar and 298 K	21	42	24	25

[a] $m^2 g^{-1}$; [b] $cm^3 g^{-1}$; [c] mmol g^{-1}; [d] kJ mol^{-1}; [e] °C

References

[1] Hu Z, Wang Y, Zhao D. Modulated Hydrothermal Chemistry of Metal–Organic Frameworks. Acc. Mater. Res. 2022;3:1106-14.

[2] Hu Z, Nalaparaju A, Peng Y, Jiang J, Zhao D. Modulated hydrothermal synthesis of UiO-66(Hf)-type metal–organic frameworks for optimal carbon dioxide separation. Inorg. Chem. 2016;55:1134–41.

[3] Hu Z, Castano I, Wang S, Wang Y, Peng Y, Qian Y, et al. Modulator effects on the water-based synthesis of Zr/Hf metal−organic frameworks: quantitative relationship studies between modulator, synthetic condition, and performance Crys.t Growth. Des. 2016;16:2295-301.

[4] Hu Z, Peng Y, Kang Z, Qian Y, Zhao D. A modulated hydrothermal (MHT) approach for the facile synthesis of UiO-66-type MOFs. Inorg. Chem. 2015;54:4862-8.

[5] Fei H, Shin J, Meng YS, Adelhardt M, Sutter J, Meyer K, Cohen SM. Reusable Oxidation Catalysis Using Metal-Monocatecholato Species in a Robust Metal–Organic Framework. J. Am. Chem. Soc. 2014;136:4965-73.

[6] Rowsell JLC, Yaghi OM. Effects of functionalization, catenation, and variation of the metal oxide and organic linking units on the low-pressure hydrogen adsorption properties of metal-organic frameworks. J. Am. Chem. Soc. 2006;128:1304-15.

[7] Myers AL, Prausnitz JM. Thermodynamics of mixed-gas adsorption. AIChE J. 1965;11:121-7.

[8] Hu Z, Wang Y, Farooq S, Zhao D. A highly stable metal-organic framework with optimum aperture size for CO_2 capture. AIChE J. 2017;63:4103-14.